JACS
JOURNAL OF THE AMERICAN CHEMICAL SOCIETY

Article

pubs.acs.org/JACS

Scanning Electrochemical Microscopy Study of Ion Annihilation Electrogenerated Chemiluminescence of Rubrene and $[Ru(bpy)_3]^{2+}$

Joaquín Rodríguez-López, Mei Shen, Alexander B. Nepomnyashchii, and Allen J. Bard*

Center for Electrochemistry, Department of Chemistry and Biochemistry, University of Texas at Austin, 1 University Station, A5300, Austin, Texas 78712-0165, United States

Supporting Information

ABSTRACT: Scanning electrochemical microscopy (SECM) was used for the study of electrogenerated chemiluminescence (ECL) in the radical annihilation mode. The concurrent steady-state generation of radical ions in the microgap formed between a SECM probe and a transparent microsubstrate provides a distance-dependent ECL signal that can provide information about the kinetics, stability, and mechanism of the light emission process. In the present study, the ECL emission from rubrene and $[Ru(bpy)_3]^{2+}$ was used to model the system by carrying out experiments with the SECM and light-detecting apparatus inside an inert atmosphere box. We studied the influence of the distance between the two electrodes, *d*, and the annihilation kinetics on the ECL light emission profiles under steady-state conditions, as well as the ECL profiles when carrying out cyclic voltammetry (CV) at a fixed *d*. Experimental results are compared to simulated results obtained through commercial finite element method software. The light produced by annihilation of the ions was a function of *d*; stronger light was observed at smaller *d*. The distance dependence of the ECL emission allows the construction of light approach curves in a similar fashion as with the tip currents in the feedback mode of SECM. These ECL approach curves provide an additional channel to describe the reaction kinetics that lead to ECL; good agreement was found between the ECL approach curve emission profile and the simulated results for a fast, diffusion-limited second-order annihilation process ($k_{ann} > 10^7$ M^{-1} s^{-1}). In the CV mode at fixed distance, the ECL emission of rubrene showed two distinct signals at different potentials when fixing the substrate to generate the radical cation and scanning the tip to generate the radical anion. The first signal (pre-emission) corresponded to an emission well before reaching the generation of the radical anion and was more intense on Au than on Pt. The second ECL signal showed the expected steady-state behavior from the second-order annihilation reaction and agreed well with the simulation. A comparison of the emission obtained with rubrene and $[Ru(bpy)_3]^{2+}$ to test the direct formation of lower energy triplets directly at the electrode showed that triplets are not the cause of the pre-emission observed. Wavelength selection experiments for the rubrene system showed that the pre-emission ECL signal also appeared slightly red-shifted with respect to the main luminophore emission; a possible explanation for this phenomenon is inverse photoemission, where the injection of highly energetic holes by the oxidized species into the negatively biased tip electrode causes emission of states in the metal that appear at a different wavelength than the singlet emission from the ECL luminophore.

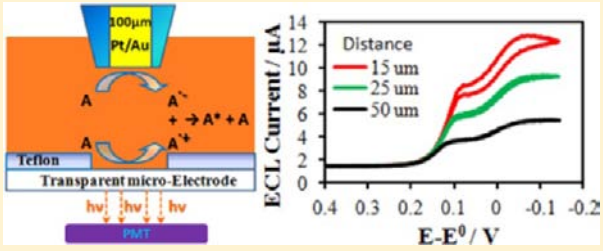

INTRODUCTION

We report the use of scanning electrochemical microscopy (SECM) for the study of the electrogenerated chemiluminescence (ECL) arising from the concurrent steady-state generation and reaction of the reactive species of two model compounds, rubrene and $[Ru(bpy)_3]^{2+}$, in MeCN−benzene and MeCN media, respectively. Direct ion annihilation, the simplest mechanism of ECL, consists of light emission from an excited state of a molecule that is produced by the electron-transfer reaction between the oxidized (e.g., a radical cation) and the reduced (e.g., a radical anion) forms of the same molecule; this reaction is exergonic enough to populate the emitting excited state of the molecule. In most ECL studies, generation of the reactive species is carried out in a transient mode by applying alternately a positive and a negative potential on a single electrode; in the present study, the radical ions are produced separately at a SECM tip and at a transparent substrate electrode through which the light generated by the reaction of such radical ions can be collected and analyzed.

ECL studies have been of interest because ECL shows a unique excitation process, particular manifestations of the effects of high-energy dissipation mechanisms in solution, and because ECL has important analytical, including commercial, applications.[1] In this study we make use of SECM, which has proven to be a superior electroanalytical tool for the study of a wide variety of electrochemical and kinetic problems.[2] In particular, we exploit its ability to generate the relevant species for annihilation ECL under steady-state conditions at two different electrodes (the oxidant at one and the reductant at the

Received: January 31, 2012
Published: May 15, 2012

   dx.doi.org/10.1021/ja301016n | *J. Am. Chem. Soc.* 2012, 134, 9240−9250

other) independently and simultaneously with control in the interelectrode spacing, d. Early attempts to study annihilation ECL by controlling the gap between the electrodes have lacked the required control of d to confirm the correspondence between experiment and the predicted ECL response and to bring d down to very small levels.[3,4]

The use of a tool such as the SECM through its precise control of the location and separation between electrodes can yield quantitative information about the kinetics of the reaction and its mechanism. In this work we demonstrate the influence of d on the ECL emission and of the kinetics of the annihilation reaction on the light emission profiles under the steady-state conditions through the efficient systems rubrene and $[Ru(bpy)_3]^{2+}$. The homogeneous second-order kinetics in which the reactants are generated at separate electrodes in the SECM has been studied under other conditions.[5] Other SECM studies of homogeneous second-order reaction mechanisms include those supported at liquid−liquid interfaces[6] and the study of rapid dimerization processes,[7,8] where rate constants up to 4×10^8 M^{-1} s^{-1} are accessible for typical solution conditions and micrometric tip−substrate gaps.

Mechanistic information on ECL has been reported previously through the use of methods that operate at steady state. The first approach used the rotating ring disk electrode for studies where positive and negative ions were formed separately on the ring and disk.[9−11] Information about the stability of the system and quantum yield of ECL was obtained by this technique. The other approach is with two closely spaced electrodes,[4,12] e.g., a thin-layer flow cell, obtaining the ECL intensity dependence on the gap size. The gap separation calculations and experimental conditions in this case are fairly tedious and lack the versatility and range offered by SECM. A related approach consists of the use of microband electrodes,[13] where light is generated by the production of the reactants where one band behaves as a cathode and the other as an anode. The production of light by annihilation appears between these spaced microelectrodes under flow conditions. In our case, steady-state conditions are reached without stirring, and d is precisely controlled, making the system more applicable for quantitative and mechanistic studies. Moreover, with SECM approach geometry, the collection efficiency is much higher than in other techniques.[14] A related study has shown that it is also possible to address the microband configuration using a confocal microspectrometer, which probes solution volume elements where ECL emission is produced.[15,16]

SECM-ECL studies can, in principle, determine the rate of the annihilation process. Annihilation ECL follows second-order kinetics, and the process is very fast.[9,17] Most ECL experiments aimed at obtaining mechanistic details are carried out under transient conditions, where it is often difficult to obtain quantitative information because of factors like double-layer charging rates. Some ECL experiments have been done under fast-scan cycling or by short pulses using chronoamperometry. A successful approach performs ECL measurements at ultramicroelectrodes under high-frequency conditions.[18−20] The determined rate constants for the annihilation reaction in highly efficient systems were of the order of 10^9−10^{10} M^{-1} s^{-1}. These studies, however, pose technical complications such as the consideration of charging currents in the short transients and the possibility of quenching by energy transfer between the electrode and the excited states formed at the very narrow diffusion layers produced by the transients. There are also indirect ways to elucidate the rate of the reactions by assuming that there is some information about different pathways.[21−23] In this case it is necessary to know the quantum yield and triplet- and singlet-state parameters. These methods appear to be sufficiently difficult that they have not been widely used.

The use of digital simulations, such as the ones provided by commercial finite element software, like COMSOL Multiphysics, allows one to obtain quantitative information about ECL mechanisms[24,25] and has already been used to model SECM systems accurately.[2,14] SECM is a good technique to determine fast rate annihilation constants because there is a continuous flow of the diffusing species in the system, and, as shown later, the annihilation reaction happens in a diffusion front away from the electrodes.[5] Our group has previously probed selected ECL systems with SECM, in the presence of a co-reactant or by generating light only at the tip by continuous cycling or stepping.[26−28] These studies focused mainly on use of the tip as a light source and optical imaging. SECM has been used for the description of co-reactant ECL from the $[Ru(bpy)_3]^{2+}$−oxalate system supported on a liquid−liquid interface.[29]

In this work we chose two well-known ECL compounds with high ECL efficiency, rubrene and tris(2,2′-bypyridine)-ruthenium(II) ($[Ru(bpy)_3]^{2+}$).[11,30] The latter has been used in applications because its solubility in water makes biological applications possible.[1,31−33] Rubrene is a typical representative of the hydrocarbon family of compounds with high ECL efficiency and has been studied for many years. Rubrene produces ECL light through both the singlet and triplet−triplet annihilation routes, while $[Ru(bpy)_3]^{2+}$ only emits via its charge-transfer (triplet-like) state.

EXPERIMENTAL SECTION

Chemicals. $[Ru(bpy)_3]Cl_2$, rubrene (≥98%), electrochemical grade supporting electrolyte tetra-*n*-butylammonium hexafluorophosphate ($TBAPF_6$), and anhydrous solvents acetonitrile (99.93%) and benzene (99.8%) were obtained from Sigma-Aldrich Co. (Milwaukee, WI) and used as received.

Electrodes. 100 μm diameter gold (99.99+%) wire from Goodfellow (Devon, PA) was used to prepare the SECM tips. The gold wire was sealed in a soft glass capillary (Frederick Haer & Co., Bowdoinham, ME) by procedures reported elsewhere.[2] The SECM tip had a radius a = 50 μm and RG of approximately 3. ITO-coated glass slides (1 mm thick) with a resistance of 10 Ω/□ and approximate transmittance of 85% from Nanocs (New York, NY) were used for the fabrication of the substrates. These were made by selectively insulating the ITO face of the glass slide with a PTFE coating in order to create a single hole that acted as a transparent microelectrode by a modification of a previously reported procedure.[34] Typical holes had a radius b = 150 μm. In all experiments, a silver wire (Goodfellow, 99.99+%) was used as a quasireference electrode. The separation between the anodic and cathodic processes of the parent molecule acts as an internal reference for calibration of the quasireference. Drifting of the reference was not observed to exceed 20 mV during the whole experimental time. The counter electrode was a 0.5 mm diameter tungsten wire from Alfa Products (Danvers, MA). The counter electrode was positioned in the SECM cell so as to block it from facing the light detector. All electrodes and the SECM cell were sonicated in acetone and dried before experiments.

Apparatus and Methods. All the solutions were prepared in an Ar atmosphere glovebox (Vacuum Atmospheres Corp., Hawthorne, CA), sealed in an airtight container, and transported to another glovebox with the SECM apparatus.

Electrochemical control of the cell and of the positioning of the electrodes was achieved using a CHI900 SECM station (CH Instruments, Austin, TX). Alignment of the SECM tip and the substrate was achieved using generation−collection techniques

described elsewhere,[2,35] with the molecule of interest serving as a mediator to avoid any contamination issues or disturbing the geometry of the setup; the closest approach distance for a well-aligned substrate is estimated as 2 μm. All approach curves were taken at an approach speed of 2 μm/s. Cyclic voltammetry (CV) was carried out at different tip−substrate gaps at 10 mV/s, which afforded steady-state response at the SECM tip. All electrochemical and positioning routines were done in the SECM station while the light responses were simultaneously acquired through a photomultiplier tube placed below the SECM cell (PMT, Hamamatsu, R4220p, Japan) and recorded using an Eco Chemie Autolab PGSTAT30 potentiostat (Utrecht, The Netherlands) interfaced through a Keithley electrometer (model 6517, Keithley Instruments Inc., Cleveland, OH). The PMT was supplied with −750 V from a Kepco (New York, NY) or a Bertan series-225 high-voltage power supply (Bertan High Voltage Corp., Hucksville, NY). ECL experiments inside an Ar drybox were done using a PMT with extended detection into red wavelengths (Hamamatsu, H9656-20) and powered through an Agilent (Santa Clara, CA) power supply. Figure 1 shows a schematic of the cell setup.

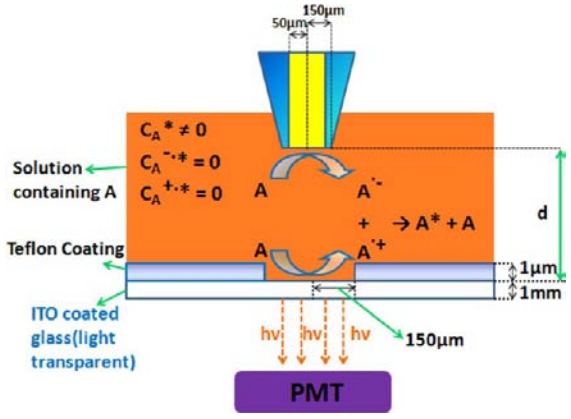

Figure 1. Schematic of the geometry and conditions used for SECM-ECL experiments using the SECM tip as radical anion generator and the transparent, selectively insulated ITO substrate as the radical cation generator. "A" represents rubrene, and the solution was 1:1 MeCN−benzene containing 0.1 M $TBAPF_6$.

RESULTS AND DISCUSSION

Simulation Results. Digital simulations of the coupled homogeneous kinetic and diffusive problem required to describe the SECM-ECL response were modeled with COMSOL Multiphysics software v3.2 for a 2-D space with axial symmetry represented through variables r and z. A complete description of the simulation model can be found in the Supporting Information, Scheme 1. Figure 2a shows a typical simulation result for the SECM-ECL system in which the radical anions produced at the tip (a = 50 μm, RG = 3) and the radical cations produced at the substrate (b = 150 μm) at steady state and under diffusion-limited conditions react rapidly (i.e., at diffusion-limited conditions) in the interelectrode gap to emit light and regenerate the parent molecule. The changes in the concentration of the parent molecule reveal clearly the formation of a reaction front located approximately midway between the tip and substrate. Figure 2 shows as well a more generalized situation in which the numbering of each concentration profile in panel c represents a position in the ECL intensity CV shown in panel b. Position 5 indicates the situation in which both the tip and substrate operate at a diffusion-limited rate and, thus, account for the system response under the conditions of an annihilation ECL approach curve. The zoomed-in interelectrode concentration profiles for this case, shown in Figure 2c for the parent molecule, radical anion, and radical cation, and the pseudoconcentration profile for the emitted light show that ECL emission occurs mainly at the reaction front created by the radical anion and cation, away from either electrode surface. The parent molecule is regenerated at this reaction front and generates an increased flux toward both electrodes, which has the effect of compressing their diffusion layers and generating a feedback current from them.[5] The fact that the parent molecule, and thus the excited state, is generated at this reaction front away from the electrode surfaces implies that quenching through energy transfer to the electrodes is probably not relevant for this configuration, when the second-order annihilation kinetics are fast. Likewise, depletion of radical ions at this reaction front should decrease importantly the effects of radical ion quenching of the excited states.

Positions 1−4 in Figure 2b,c show in more detail the establishment of the diffusion-limited reaction front. Ion annihilation ECL is not observed significantly at position 1, since at the tip potential no significant production of radical anions is observed; in this case, collection of the radical cation occurs at the tip electrode and the parent molecule is regenerated at a large overpotential. In position 2, small amounts of the radical anion are formed and the annihilation ECL process starts; at this stage, the diffusion layer for the formation of the parent molecule has not become significantly detached from the tip electrode. This detachment is more evident from position 3 and onward. Electrode effects could be relevant in the ECL emission in positions 1 and 2, but not afterward, when the concentration profile for the parent molecule and excited state has been pushed into the interelectrode gap. A discussion of possible effects is given in the Experimental Section for CV.

Figure 3 shows the effect of the annihilation reaction on the SECM approach curves and voltammetry with electrodes approached to different distances to the substrate. Figure 3a shows the predicted differences between a typical SECM approach curve (e.g., production of radical anion at the tip and regeneration to parent molecule at the substrate) and the annihilation approach curve, i.e., tip electrode producing radical anion and substrate electrode producing radical cation and reaction in the interelectrode gap. The simulations shown in Figure 3a are in agreement with previous studies that showed that the increase in feedback current due to the production of an additional electroactive or reacting species at the substrate is independent of the value of the second-order reaction constant between the tip-generated and substrate-generated species, i.e., annihilation.[5] A compensation effect, in which lack of chemical reaction in the interelectrode gap is replaced by collection of the oxidized species at the tip electrode is always operative and generates an increased current at the tip which is constant in magnitude, regardless of the values of k_{ann}; e.g., the red curve in Figure 3a is always the same as long as the substrate operates under steady-state, diffusion-limited conditions. Figure 3b shows instead that the ECL response approach curves do exhibit a dependence on the second-order rate constant k_{ann}, and that as the diffusive flux of the species is increased upon bringing the electrodes together, high rate constants (e.g., close to diffusion limitation) yield larger ECL intensities; on the other hand, lower rate constants are unable to compete with the increase in the precursor redox recycling at the electrodes (i.e., collection of the radical cation at the tip and conversely, of

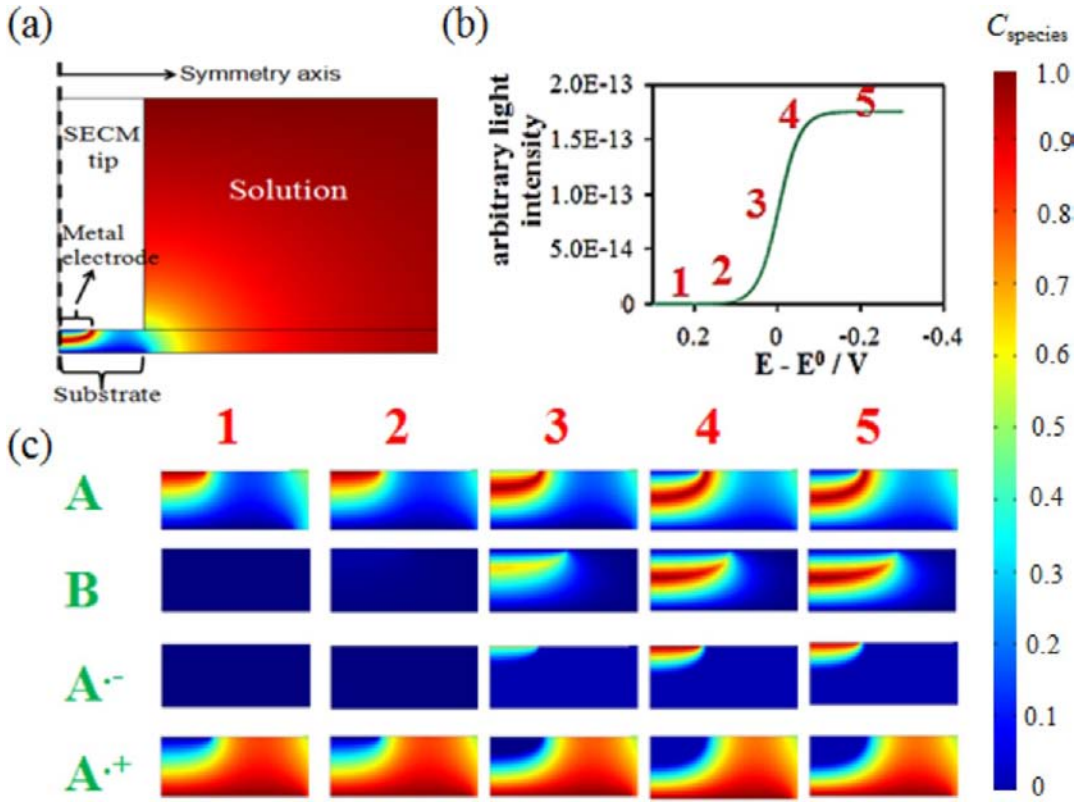

Figure 2. Simulation results for SECM-ECL in the CV mode at d = 50 μm. (a) General concentration profile for the parent molecule A at steady state under diffusion-limited conditions at both the tip and substrate following the geometry described in the simulation model. (b) Light intensity resulting from tip CV with resulting annihilation in the tip−substrate gap with the substrate operating at diffusion-limited steady state; regions marked correspond to the tip−substrate gap concentration profile shown in (c), where these profiles are shown for the parent molecule A, the corresponding radical ions, and the light-emitted B, treated as a pseudoparticle. The substrate generates $A^{\bullet+}$ at a diffusion-controlled rate and the tip scanned toward $A^{\bullet-}$ production as shown in (b). Concentration scale applies to molecular species, and for them $D = 1 \times 10^{-5}$ cm^2/s. Parent molecule bulk concentration C_A = 1 mM.

the radical anion at the substrate) and the ECL intensity drops as the electrodes are brought together. Under these conditions the radical ions reach the electrodes where they are converted and pass by each other without reacting, thus not generating ECL.

Figure 3c shows the steady-state voltammetry of the system at different d values; as expected, before the tip reaches the standard reduction potential of the parent molecule, the tip shows an offset current that corresponds to the collection of the radical cation produced at the substrate. This collection increases as the electrodes are brought more closely together due to an increase in the collection efficiency.[14] Past the reduction potential of the parent molecule, there is an increase in the current due to the triggering of the annihilation reaction in the interelectrode gap. This increase in current produces the ECL, with simulated results shown in Figure 3d. Since the collection of the radical cation at the tip generally does not result in emission, the profile of the light emission follows the profile of the electrochemical generation of the radical anion. Plateau ECL currents increase with decreasing distance, as expected from the ECL approach curves in Figure 3b. In principle, at a sufficiently small d, the ECL emission should decrease because the diffusional flux of the ions becomes larger than the annihilation reaction can sustain at a given k_{ann}.

EXPERIMENTAL RESULTS

The Rubrene System. We performed SECM-ECL experiments with the efficient ECL emitter rubrene. Rubrene is considered an ECL standard, with a reduction potential E^0_{red} = −1.41 V vs SCE and oxidation potential E^0_{ox} = 0.83 V vs SCE. It fluoresces at λ_{max} = 563 nm and has an overall ECL efficiency of 0.05%.[1] It forms a singlet excited state with energy 2.2 eV and a triplet with 1.1 eV and can produce ECL through the S-route or via triplet−triplet annihilation (T-route).[36] Figure 4a shows its reversible CV for both oxidation and reduction at the SECM tip (a = 50 μm) under transient conditions, while Figure 4b shows its oxidation at the transparent ITO electrode (which was never biased negatively to avoid its degradation). The tip and substrate electrodes were co-aligned using previously reported procedures that rely on a combination of feedback and collection modes of SECM.[5,35] Figure 4c shows the chemically and electrochemically reversible production of the necessary species for ECL through CV in the tip generation−substrate collection mode of SECM. Here, the substrate collects and recycles the products of the tip (either the radical anion or cation); the high collection efficiency of the system indicates chemical stability of these species, while the symmetry and magnitude of the currents at tip and substrate indicate a fast and reversible electrode reaction at both tip and substrate. These characteristics are well reproduced in the goodness of the fit for the approach curve shown in Figure 4d, where the radical anion was produced at the tip and oxidized at the

dx.doi.org/10.1021/ja301016n | J. Am. Chem. Soc. 2012, 134, 9240−9250

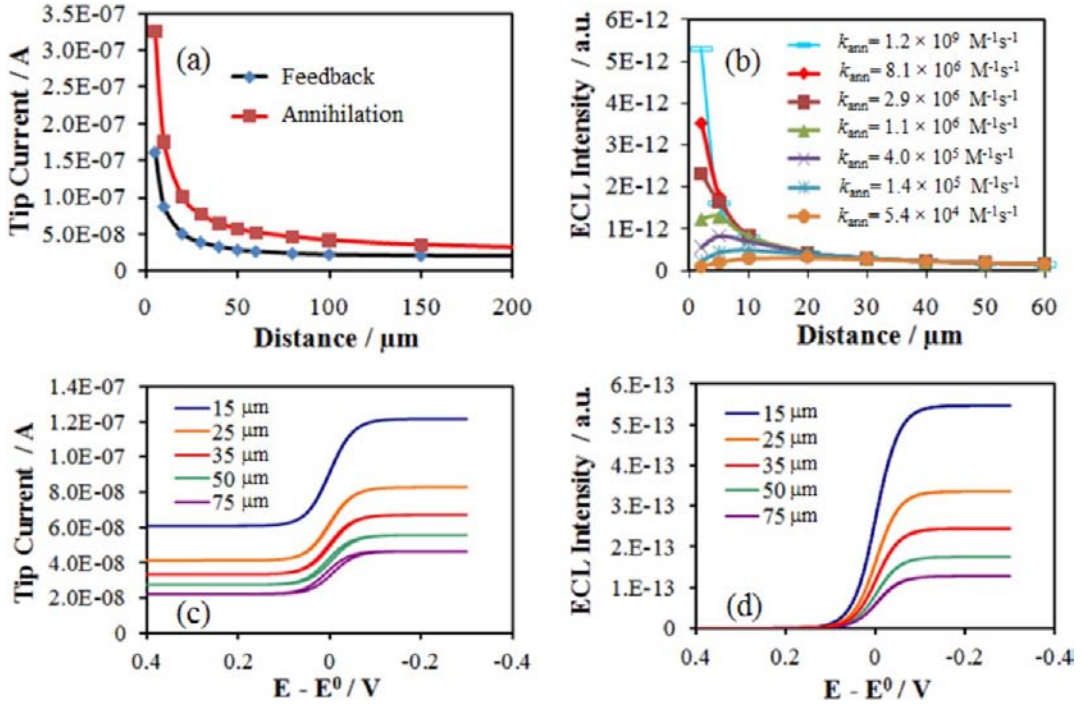

Figure 3. Simulated results for SECM-ECL under the conditions described in the Supporting Information, Scheme 1. All molecular species, $D = 1 \times 10^{-5}$ cm^2/s, parent molecule bulk concentration $C_A = 1$ mM. (a) Approach curve comparison when the tip operates in conventional feedback mode generating the radical anion and when the substrate generates the reactive radical cation. (b) ECL intensity profiles for different values of the reaction constant k_{ann} for the system described in (a). (c) Electrochemical tip responses for different tip−substrate distances, d, when the annihilation reaction operates at diffusion-limited conditions. (d) Light intensity CV profiles corresponding to (c).

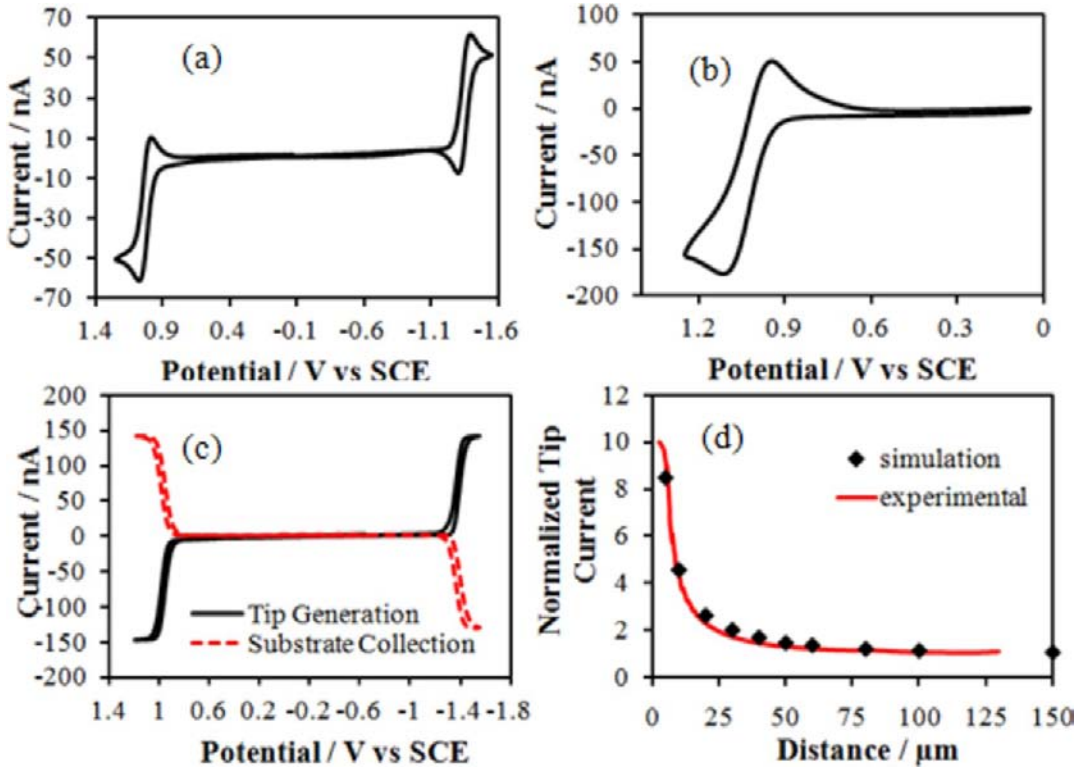

Figure 4. Experimental behavior of rubrene at the tip and substrate, C* = 1 mM in benzene/acetonitrile 1:1 solution, 0.1 M $TBAPF_6$. (a) Complete CV at the Au tip (a = 50 μm, ν = 100 mV/s). (b) CV for the oxidation process at the ITO substrate electrode (b = 150 μm, ν = 100 mV/s). (c) Verification of the tip−substrate alignment and of chemical stability of the electrogenerated species by tip generation−substrate collection experiments at fixed height. (d) Tip feedback approach curve for radical anion production at tip with substrate biased at 0 V vs SCE.

dx.doi.org/10.1021/ja301016n | J. Am. Chem. Soc. 2012, 134, 9240−9250

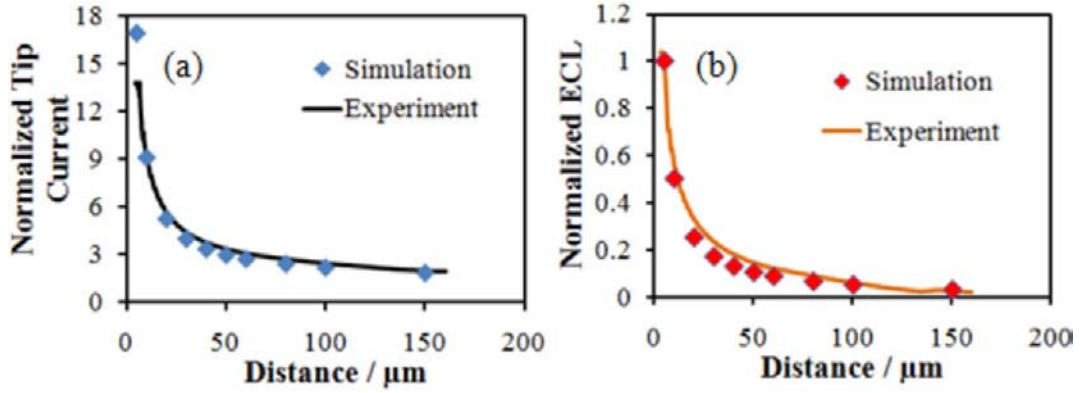

Figure 5. Radical annihilation approach curves for rubrene with electrode reactions proceeding under diffusion-limited conditions: (a) tip electrochemical feedback approach curve and (b) light emission profile, normalized with respect to the intensity at closest approach, d, at 5 μm.

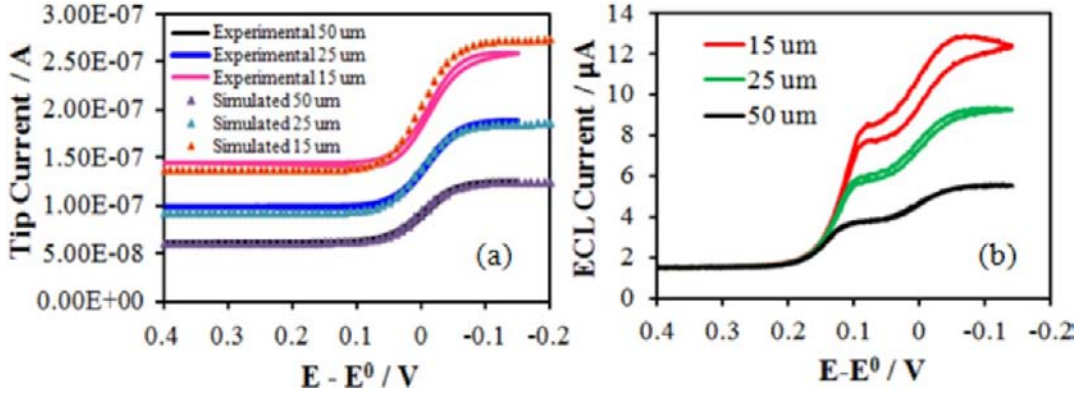

Figure 6. Radical annihilation CV curves at different distances for rubrene with substrate electrode reaction proceeding under diffusion-limited conditions and the tip potential scanned at ν = 10 mV/s (a) Tip electrochemical feedback CV curves and (b) corresponding light emission CV curves. E^0 refers to the reduction process at E^0 = −1.41 V vs SCE.

substrate. The anhydrous and inert conditions of the glovebox allow us to obtain an approach curve devoid of chemical complications that could be present with the generation of reactive rubrene radical ions, $R^{\bullet+}$ and $R^{\bullet-}$, as in this experiment. Furthermore, the use of a well-sharpened tip and the choice of tip and substrate size provided a good compromise between detected ECL intensity and reasonable approach distances, where normalized $L = d/a$ values of $L \approx 0.1$ were common.

Rubrene Annihilation Approach Curves. Once the electrodes were aligned and conventional feedback approach curves as well as voltammograms were obtained to ensure the stability of the system, annihilation approach curves, generating $R^{\bullet-}$ at the tip and $R^{\bullet+}$ at the substrate, could be run in the dark while simultaneously recording the electrochemical tip current and the ECL response from the photomultiplier tube. Figure 5 shows such results for the tip current and the ECL signal. In this case both electrodes were biased at potentials where the steady-state, diffusion-limited production of $R^{\bullet-}$ (at the tip) and $R^{\bullet+}$ (at the substrate) holds and approached from large interelectrode distances to shorter ones at a slow scan rate (e.g., 1 μm/s). The fit of the experimental data to the simulations, as shown in Figure 5 for both electrochemical and spectroscopic channels, is good evidence of the cleanliness of the system, which yields a stable steady-state ECL emission. In this case, the fit obtained to the ECL annihilation curves at the distances probed and, according to Figure 3 b, is consistent with $R^{\bullet-}$ + $R^{\bullet+}$ annihilation rate constants of the order of $k_{ann} \geq 1 \times 10^7$ M^{-1} s^{-1}. This result is consistent with those reported from a transient technique using high-frequency waveforms on microelectrodes for other ECL luminophores such as 9,10-diphenylanthracene, dimethylanthracene, and ruthenium(II) tris-bipyridine in MeCN, where $k_{ann} \geq 1 \times 10^{10}$ M^{-1} s^{-1} was reported.[19,20] While the SECM method and the interelectrode distance used here cannot access these higher rate constants, it did provide steady-state, reproducible approach curves that fit well to theory both electrochemically and spectroscopically in comparison to other approaches to bringing electrodes into close proximity, as described in the Introduction. Moreover, the fit of the approach curves of this model ECL luminophore to the expected results is a first step toward the study of other effects on its ECL emission. Higher rate constants can be accessed by decreasing d,[7,37] although this was not further probed in these experiments. ECL measurements allow a secondary channel to measure kinetics in the gap between tip- and substrate-generated species where the reversibility of the system prevents measurement of kinetics. A study of this ECL emission phenomenon as a function of tip potential, however, produced an unexpected response, as shown in the following sections.

ECL During Voltammetry. Figure 6 shows the tip voltammograms of the SECM-ECL system for rubrene using a Au tip at different interelectrode distances, d, and the ECL signal. The electrochemical current fits very well with the simulation model; the collection characteristics of the system (e.g., prior to the reduction wave), which are importantly dependent on RG,[14] are well reproduced experimentally, as well

dx.doi.org/10.1021/ja301016n | J. Am. Chem. Soc. 2012, 134, 9240−9250

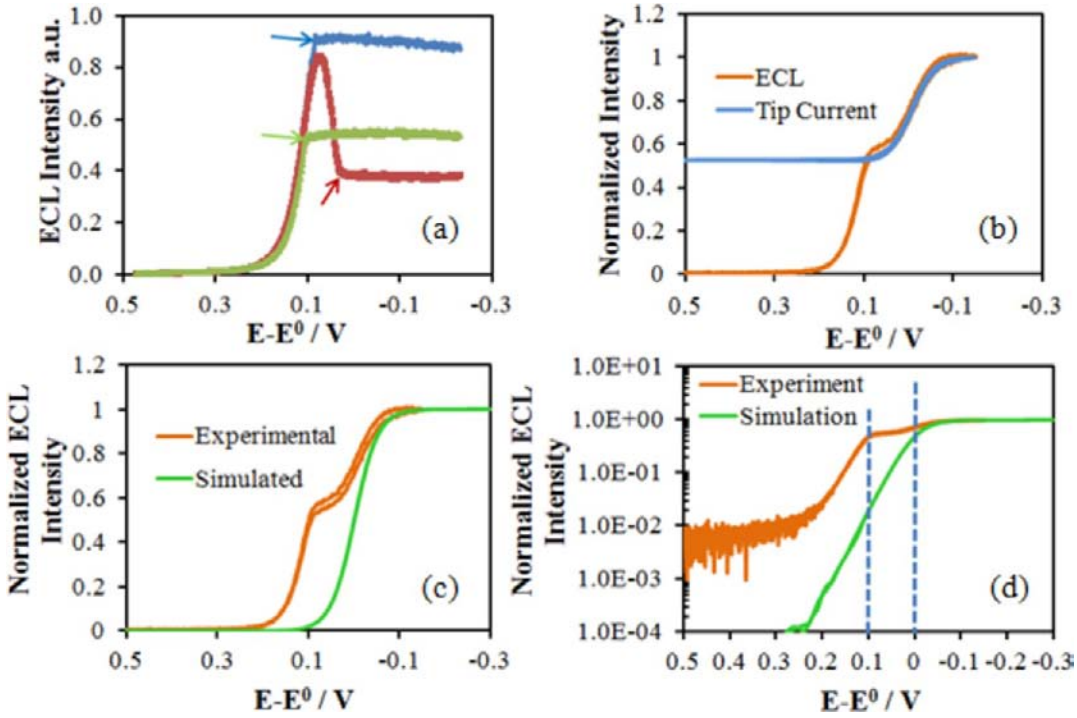

Figure 7. Comparison between simulated and experimental light CV profiles at d = 25 μm and tip scan rate ν = 10 mV/s. (a) Demonstration of the steady-state nature of light in pre-wave region by stopping the CV scan at the points indicated by the arrows; in the indicated steady emission region the potentials are held constant for times corresponding to 10 s per 0.1 V marker. (b) Comparison between tip current and ECL emission showing the appearance of the second ECL process along the production of the radical anion at the tip. (c) Comparison between the simulated and experimental ECL profile; (d) same as (c) but in logarithmic scale (base 10). E^0 refers to the reduction process at E^0 = −1.41 V vs SCE.

as the electrochemically reversible steady-state reduction wave that corresponds to the generation of the radical anion. In contrast, the ECL CV shows the appearance of two overlapping curves, as shown in Figure 6b. The first wave, at the less negative potentials, occurs at potentials of about 0.2 V before the onset of the electrochemical reduction wave, i.e., where only about 0.1−1% of the parent R or $R^{\bullet+}$ is converted to $R^{\bullet-}$. The emission at more negative potentials occurs where the reduction of wave for R occurs; the emission at both waves increases with decreasing distance as observed with the approach curves. This emission pre-wave changed slightly from experiment to experiment, sometimes showing a more peak-like appearance, but was always present and in a similar proportion to the second wave in different experiments. The increase in the light emission for the pre-wave showed good correspondence to the increase in radical cation collection by the tip with decreasing d (Supporting Information, Figure S1).

The pre-wave ECL emission remained constant at a given potential when the scan was stopped as shown in Figure 7a. Thus recording a voltammogram and then holding both tip and substrate potentials constant during the scan at selected potentials, the ECL (and electrochemical) signal were steady at a constant emission level. This implies that transient effects such as adsorption of products or reactants at the electrode surface, for which transient adsorption peaks could be invoked, is not the underlying cause of this emission. The correspondence of the electrochemical reduction wave to the emission process at more negative potentials can be better appreciated in Figure 7b, where the expected sigmoid profile for the current can be clearly observed for these processes. Figure 7c shows the light emission profile compared to the simulated one for the S-route $R^{\bullet-}$ + $R^{\bullet+}$ reaction, in which the emission pre-wave is more evident. In the region of the pre-wave the level of current above the background $R^{\bullet+} \rightarrow R$ current is small. Figure 7d shows, however, upon closer inspection with emission plotted on a logarithmic scale, that ECL is emitted at tip potentials well below the standard reduction potential of rubrene, where very small but finite current flows, as calculated from the Nernst equation. A comparison of the experimental to the simulated case on this scale shows a corresponding linear decay process of the ECL intensity that has approximately the same slope for the experimental and simulated cases, but the experimental case shows the additional pre-annihilation process at potentials within about 0.2 V from the potential for reduction of rubrene as an additional process that affects the ECL intensity.

As discussed earlier, the rubrene system has been shown to proceed through production of triplets followed by triplet−triplet annihilation, the T-route, especially when the annihilation reaction involves a reactant, like tetra-*n*-methyl-*p*-phenylene diamine radical cation, that is of insufficient energy to produce the rubrene singlet. This model has been reinforced by studies of the magnetic field effect on the emission.[38] That is, on energetic grounds the direct formation of the singlet excited state from the rubrene radical ions is marginally possible, because the difference between the standard reduction and oxidation potentials is 2.24 eV, which when adjusted for the estimated entropy contribution of ∼0.1 eV yields an annihilation energy of ∼2.14 eV (compared to the energy for formation of the singlet, ∼2.2 eV). The formation of the triplet state with an energy of ∼1.1 eV is energetically more favorable. In the early days of the development of ECL it was also proposed that the formation of excited states through a so-called pre-annihilation route, in which an excited state was

dx.doi.org/10.1021/ja301016n | J. Am. Chem. Soc. 2012, 134, 9240−9250

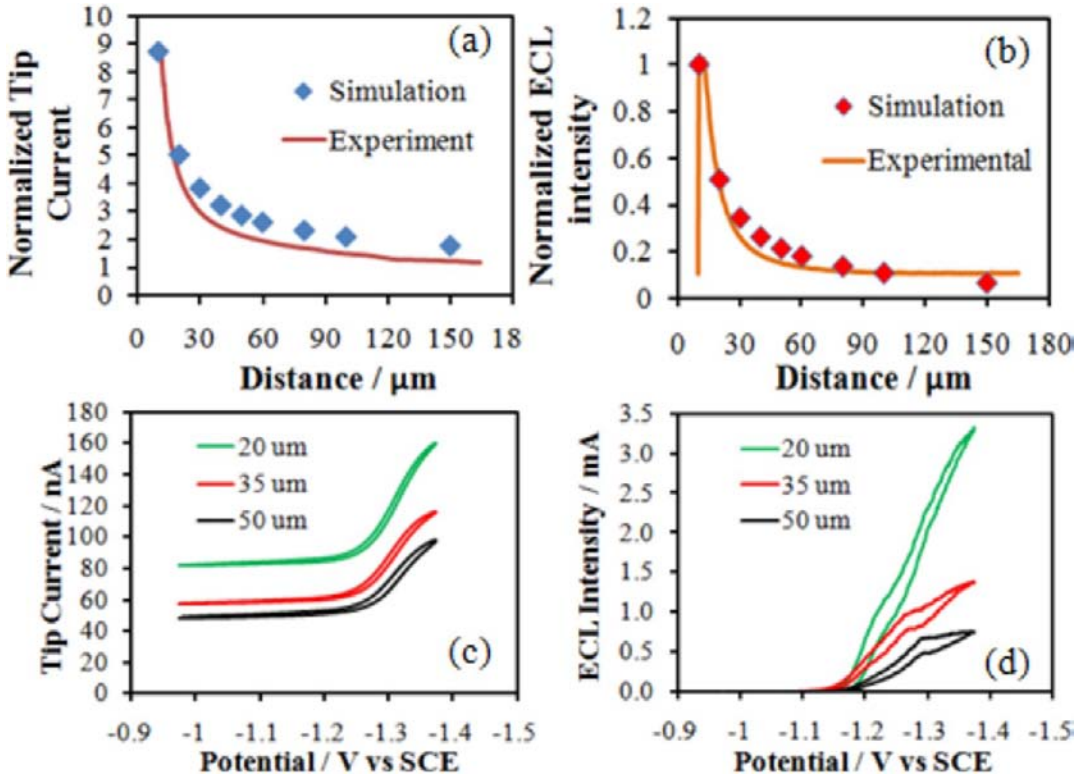

Figure 8. SECM-ECL results for 1 mM $[Ru(bpy)_3]^{2+}$ in MeCN with 0.1 M $TBAPF_6$ as supporting electrolyte. (a) Annihilation approach curve (tip current) for both electrodes working at diffusion-limited conditions. (b) ECL approach curve for the case in (a), normalized to the intensity of closest approach. (c) Annihilation in the CV mode, with substrate operating at diffusion-limited conditions and tip voltammetry at ν = 10 mV/s. (d) Corresponding ECL emission curves for (c).

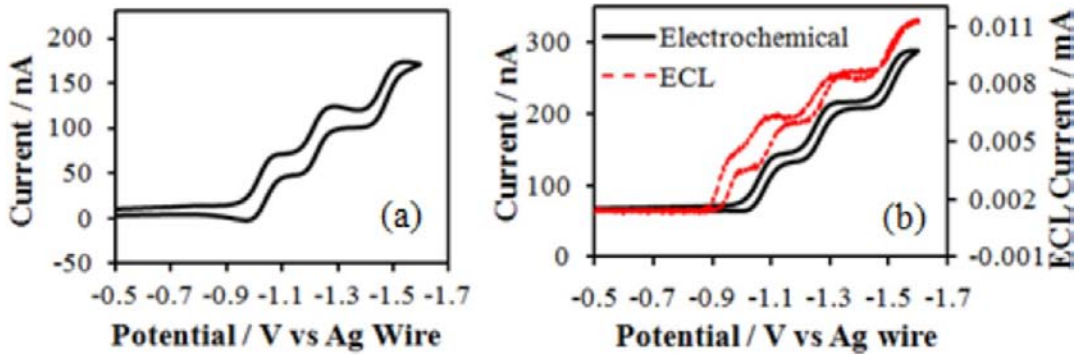

Figure 9. SECM-ECL voltammetry of the system $[Ru(bpy)_3]^{2+}$. (a) Reduction of ~1.4 mM $[Ru(bpy)_3]^{2+}$ at the Au tip and at very large tip–substrate separations, scan rate 50 mV/s. (b) Electrochemical reduction and corresponding ECL emission profile with the tip and substrate separation of 50 μm, scan rate 50 mV/s.

generated through direct electron transfer from the electrode into a species in solution, is possible,[39−41] e.g., in our case, from the reduction of the cation radical at the Au tip electrode. This proposal was later disputed on the basis of the improbability of formation of an excited state close to the electrode surface because of energy transfer to the metal,[42] and it was proposed that pre-annihilation arose from impurities in the solutions,[43] although clean solutions of rubrene still showed some pre-annihilation at potentials close to the foot of the CV waves.[41] Note, however, that later studies,[20] including direct formation of emitting states at semiconductor surfaces, or even of adsorbed emitters on metals, have been seen. Following the rubrene energetic argument, although a singlet state could not be directly populated prior to reaching the standard reduction potential of the molecule, it would be possible to form the excited triplet state and allow for an efficient triplet−triplet annihilation mechanism to drive the formation of the singlet state. To test this hypothesis, we turned to a system in which triplet−triplet annihilation is not present and formation of only one type of excited state is possible: the efficient ruthenium(II) tris-bipyridine ($[Ru(bpy)_3]^{2+}$) ECL system.

$[Ru(bpy)_3]^{2+}$ SECM-ECL Experiments. SECM-ECL experiments were performed on the $[Ru(bpy)_3]^{2+}$ system, which shows a reversible oxidation at E^0_{ox} = 1.35 V vs SCE primarily of the Ru(II) center and three reversible reductions corresponding to each of the ligands. The first reduction process has a standard reduction potential E^0_{red} = −1.32 V vs SCE. The excited state of $[Ru(bpy)_3]^{2+}$ photoluminesces with

dx.doi.org/10.1021/ja301016n | J. Am. Chem. Soc. 2012, 134, 9240−9250

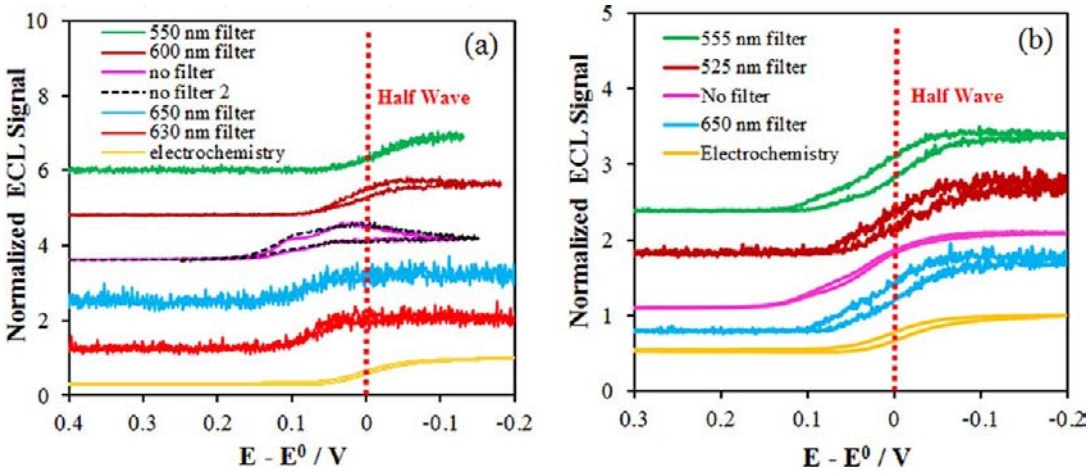

Figure 10. SECM-ECL experiments for rubrene in CV mode using dichroic filtering. Comparison of the ECL emission at different central wavelengths for each filter to the overall ECL intensity and electrochemical tip response using a long-wavelength enhanced photomultiplier tube; plots are displaced in the vertical axis for clarity. Tip electrode material was (a) polycrystalline gold or (b) polycrystalline platinum.

an emission λ_{max} = 608 nm is ascribed to a metal-to-ligand charge transfer (MLCT) with approximately 10% singlet character and 90% triplet character and an energy of 2.0 eV.[44] Because of these characteristics the excited state also has a relatively long lifetime of 0.8 μs.[44] Figure 8a,b shows that the annihilation approach curves for both current and ECL emission, corresponding to the reaction of $[Ru(bpy)_3]^+$ (produced at the Au tip) and $[Ru(bpy)_3]^{3+}$ (produced at the ITO substrate), essentially fit the predicted response for a fast system, as observed in the case of rubrene. As mentioned earlier, the direct formation of an emitting lower-energy excited state is not expected for this system, since only emission from the MLCT state is present. Figure 8c,d shows the annihilation CV profiles for tip current and ECL emission. Even with this system, however, a pre-emission peak is present well below the standard reduction potential of the complex.

The possibility that further reduced states of the complex could account for part of this pre-emission was probed; Figure 9a shows the three reductions of $[Ru(bpy)_3]^{2+}$ at the Au tip and at very large tip−substrate separations, while Figure 9b shows the electrochemical and ECL emission profile for this case with the tip and substrate at a distance of 50 μm where ECL is observed (a higher scan rate than in the steady-state case was used in here to prevent fouling of the tip at the more negative tip potentials). The pre-emission is still observed in this case, along with the ECL contribution from the three reduced species generated at the tip. The possibility that another species, e.g., oxygen, which is invariably present at low concentrations, even in the glovebox, plays a role in enhancing the ECL emission was also probed (Supporting Information, Figure S2a,b and corresponding discussion), but it only showed a quenching behavior.[45]

ECL Spectra and SECM-ECL CV Experiments at Au and Pt Electrodes. With the hope that obtaining some information about the emission wavelengths would be useful in understanding the pre-annihilation response, electrochemical SECM-ECL experiments in the CV mode were carried out in a drybox (to minimize oxygen and water contamination) with a photomultiplier tube with extended red wavelength detection used to record rubrene ECL emission. Since the response through a monochromator was too weak, interference band-pass filters were used to monitor selected wavelengths as the tip scan progressed from a potential where only collection of the radical cation is present to that of the generation of the radical anion. Figure 10 shows the spectrally resolved SECM-ECL CV for the rubrene system using an Au or a Pt tip. Although exactly the same solution conditions were used, the ECL emission profile is somewhat different with these two tip materials, suggesting that the tip material plays a role in the pre-emission behavior.

As shown in Figure 10a (Au tip), the total ECL emission of the system shows differences with respect to that shown in Figure 6b because of the use of a photomultiplier tube that is more sensitive to red wavelengths, but it also shows other characteristics. The pre-wave is followed by a slightly deformed plateau. The CV emission profiles at different central wavelengths are shown for both panels and compared to the electrochemical half-wave potential for the first rubrene reduction wave. The emission profiles for the longer wavelengths (e.g., 630 and 650 nm) in the case of the Au tip start at an earlier onset potential compared to those at the shorter wavelengths (550 and 600 nm) and reach a steady state well below the hal-wave potential, while the half-wave potential for the ECL emission for the shorter wavelengths reasonably agree with the one obtained from the electrochemical current (recall that for rubrene emission λ_{max} = 563 nm). The spectra obtained for a Pt tip, Figure 10b, show a smaller contribution of the pre-emission to the ECL signal, and in comparison of electrochemical half-wave potential to emission half-wave potential at different wavelengths, they all show a much smaller discrepancy to the simulation than those on Au. In both Au and Pt experiments, when using filters between 550 and 600 nm, i.e., close to the maximum emission wavelength, there is a good agreement between the simulated and experimental SECM-ECL CV.

Given the effect of the electrode metal on the ECL, it is tempting to explain the preannihilation by inverse photoemission.[46] In charge-transfer inverse photoemission at a metal/electrolyte interface during oxidation,[47,48] a strongly reducing species in solution injects an electron into a metallic electrode that, when biased at a sufficiently large positive overpotential injects a hole and the recombination process causes the emission of light. Alternatively during a reduction reaction, a strongly oxidizing species injects a hole that

recombines with an electron injected from the metallic contact. The λ_{max} of the emitted light depends on the difference between the potential at which the reacting species injects an electron (or a hole) and the overpotential at the electrode, with shorter wavelengths corresponding to larger potential differences. Only species with $E^0_{red} < -1.9$ V vs SCE and $E^0_{ox} > 0.86$ V vs SCE inject electrons or holes with sufficient energy to cause visible emission.[49,50] The intensity of the emission increases with increasing overpotential and is strongly dependent on the electrode material.[49,51,52] Au shows a strong inverse photoemission behavior compared to other metals such as Pt, Pd, and Rh; for example, Au(111) is reported to produce an emission 50 times larger upon hole injection than Pt.[46,47] Au also typically emits with λ_{max} below 2.3 eV (wavelengths longer than 539 nm), more red-shifted than other metals such as Pt.[51] Both surface states[49−52] and the electronic structure of the bulk metal[46,51] contribute to this difference in behavior between electrode materials; in particular, the bulk emission from Au is more intense due to a larger penetration depth of the injected charge carriers into the metal, e.g., approximately 50 nm at 2 eV for Au but only 13 nm at 2 eV for Pt.[46,51] The experiments presented in Figure 10 show the same trends expected for inverse photoemission: a larger pre-emission is observed for Au compared to that of Pt, this emission increases as the tip potential is made more negative (larger overpotential), it is observed with a molecule with $E^0_{ox} \geq 0.86$ V vs SCE (rubrene is close to this value and $[Ru(bpy)_3]^{2+}$ surpasses it), and its emission profile blue-shifts slightly at larger overpotentials as shown by the corresponding more negative half-wave potentials for ECL emission observed with shorter wavelength filters. In the case of Au, the observation that the exact shape of the emission varied from experiment to experiment (*vide infra*) can be explained perhaps by its occurrence at an electrode with a different proportion of facets and defects that could lead to slightly different surface states from experiment to experiment.

Past inverse photoemission experiments were typically conducted with electron- or hole-injecting molecules that do not exhibit ECL to avoid the interference from this emission, and all of them were carried out under transient conditions at large electrodes. However, inverse photoemission typically is very weak with an efficiency much lower than that of ECL, for instance, of the order of 1×10^{-5} % for *trans*-stilbene, benzonitrile, and benzoquinone on Pt in acetonitrile compared to the ECL efficiency of 5% for the $[Ru(bpy)_3]^{2+}$ system. While it would be difficult with the present experiments to prove that inverse photoemission could be enhanced by using an ECL luminophore, it is true that the SECM conditions used here, where the mass transfer of the reacting radical cation to the Au electrode increases as the interelectrode distance is made shorter (Supporting Information, Figure S1), could lead to an enhanced hole injection process. Notice as well that this inverse photoemission process at the tip electrode is expected to disappear as the radical anion is produced; as shown in Figure 2c, beyond the potential indicated as 3, the reaction front between the radical ions is pushed into the solution once the radical anion is produced; therefore, the hole injection process to the metal is prevented by the flux of anion radical, as in the present experiments. However, the interpretation of the experimental SECM-ECL approach curves is valid even in the presence of this effect.

Additional studies must be carried out to understand this interesting effect, which is not seen, for example, in rotating ring disk electrode ECL experiments with rubrene[9] carried out, however, only on Pt and under less rigorous conditions. Perhaps the SECM approach with different metals will be useful in testing the inverse photoemission hypothesis.

CONCLUSIONS

This study reports on the first application of scanning electrochemical microscopy to the study of electrogenerated chemiluminescence in the radical annihilation mode and under dry and inert conditions. This technique allows the study of fast electron transfer reactions and inspection of the ECL processes with unprecedented detail through a controlled two-electrode setup. In order to enhance the light collection efficiency of the system, a selectively insulated ITO-transparent substrate in the shape of a microelectrode was used to produce the radical cations and a metallic SECM tip used to produce the radical anions; these electrodes were co-aligned, and the ECL emission was obtained at different interelectrode distances. The ECL annihilation reactions, as probed by SECM and ECL approach curves, combined with digital simulation of the electrochemical and light response, are observed to follow very fast second-order homogeneous kinetics with an annihilation constant $k_{ann} > 10^7$ M^{-1} s^{-1} for the case of the rubrene and tris(bipyridine) ruthenium systems. ECL measurements allow a secondary channel to measure kinetics in the gap between an SECM tip and a substrate where the reversibility of the system prevents elucidation of reaction paths by SECM current measurements alone.[5] The presence of oxygen quenches the ECL emission of $[Ru(bpy)_3]^{2+}$ and yields annihilation approach curves with smaller apparent second-order kinetics than those for the systems in an inert atmosphere.

SECM-ECL experiments conducted in the CV mode at different tip−substrate distances showed good correspondence to the electrochemical model except an important discrepancy in the profile of the ECL emission. A strong pre-annihilation emission wave was observed at potentials before appreciable generation of radical anion at the tip. This emission was seen with both rubrene and $[Ru(bpy)_3]^{2+}$. Because the tip material, i.e., Au vs Pt, showed an important effect, these observations were rationalized in terms of the phenomenon of inverse photoemission, in which the radical cations generated at the substrate can inject holes into the biased tip and produce light emission at the metal disk at negative potentials where electron injection from the power source occurs. The inverse photoemission becomes unimportant when the fast annihilation process in the interelectrode gap takes over and the ECL process dominates, because the radical no longer directly accesses the electrode. The use of interference filters at the peak emission of the luminophore alleviates importantly the effects of the pre-emission wave and yield the expected simulated emission profile. While the SECM-ECL technique is quite challenging to carry out, the demonstration of its use for two model systems and its ability to uncover subtle effects, suggests this technique may be useful in the elucidation and understanding of ECL mechanisms (e.g., reaction kinetics, quenching and radical ion stability effects, multiple electron transfers), and possibly for the study of other related phenomena such as inverse photoemission in solution.

ASSOCIATED CONTENT

Supporting Information

Description of the simulation model, a comparison between SECM collection current and pre-annihilation intensity, and SECM-ECL experiments of $[Ru(bpy)_3]^{2+}$ in the presence of

oxygen. This material is available free of charge via the Internet at http://pubs.acs.org.

AUTHOR INFORMATION

Corresponding Author

ajbard@mail.utexas.edu

Notes

The authors declare no competing financial interest.

ACKNOWLEDGMENTS

We thank the National Science Foundation (CHE 0808927), and the Robert A. Welch Foundation (F-0021) for financial support of this research. J.R.-L. thanks Eli-Lilly and Co. for a Division of Analytical Chemistry fellowship from the American Chemical Society.

REFERENCES

(1) For reviews on ECL, see: (a) *Electrogenerated Chemiluminescence*; Bard, A. J., Ed.; Marcel Dekker: New York, NY, 2004. (b) Richter, M. *Chem. Rev.* **2004**, *104*, 3003−3036. (c) Knight, A. W.; Greenway, G. M. *Analyst* **1994**, *119*, 879−890. (d) Miao, W. *Chem. Rev.* **2008**, *108*, 2506−2553.

(2) *Scanning Electrochemical Microscopy*; Bard, A. J., Mirkin, M. V., Eds.; Marcel Dekker: New York, NY, 2001.

(3) Hercules, D. M. *Science* **1964**, *145*, 808−809.

(4) Brilmyer, G. H.; Bard, A. J. *J. Electrochem. Soc.* **1980**, *127*, 104−110.

(5) Wang, Q.; Rodríguez-López, J.; Bard, A. J. *ChemPhysChem* **2010**, *11*, 2969−2978.

(6) Mirkin, M. V.; Tsionsky, M. In *Scanning Electrochemical Microscopy*; Bard, A. J., Mirkin, M. V., Eds.; Marcel Dekker: New York, NY, 2001; Chapter 8, pp 299−342.

(7) Zhou, F.; Unwin, P. R.; Bard, A. J. *J. Phys. Chem.* **1992**, *96*, 4917−4924.

(8) Unwin, P. R. In *Scanning Electrochemical Microscopy*; Bard, A. J., Mirkin, M. V., Eds.; Marcel Dekker: New York, NY, 2001; Chapter 7, pp 241−298.

(9) Maloy, J. T.; Bard, A. J. *J. Am. Chem. Soc.* **1971**, *93*, 5968−5981.

(10) Maloy, J. T.; Prater, K. B.; Bard, A. J. *J. Am. Chem. Soc.* **1971**, *93*, 5959−5968.

(11) Tokel-Takvoryan, N. E.; Hemingway, R. E.; Bard, A. J. *J. Am. Chem. Soc.* **1973**, *95*, 6582−6589.

(12) Laser, D.; Bard, A. J. *J. Electrochem. Soc.* **1975**, *122*, 632−640.

(13) Bartelt, J. E.; Drew, S. M.; Wightman, R. M. *J. Electrochem. Soc.* **1992**, *139*, 70−74.

(14) Sánchez-Sánchez, C. M.; Rodríguez-López, J.; Bard, A. J. *Anal. Chem.* **2008**, *80*, 3254−3260.

(15) Amatore, C.; Pebay, C.; Servant, L.; Sojic, N.; Szunerits, S.; Thouin, L. *ChemPhysChem* **2006**, *7*, 1322−1327.

(16) Amatore, C.; Oleinick, A.; Klymenko, O. V.; Thouin, L.; Servant, L.; Svir, I. *ChemPhysChem* **2007**, *8*, 1664−1676.

(17) Feldberg, S. W. *J. Phys. Chem.* **1966**, *70*, 3928−3930.

(18) Collinson, M. M.; Wightman, R. M. *Science* **1995**, *268*, 1883−1885.

(19) Collinson, M. M.; Wightman, R. M. *Anal. Chem.* **1993**, *65*, 2576−2582.

(20) Collinson, M. M.; Wightman, R. M.; Pastore, P. *J. Phys. Chem.* **1994**, *98*, 11942−11947.

(21) Kapturkiewicz, A. *Chem. Phys.* **1992**, *166*, 259−273.

(22) Kapturkiewicz, A. *J. Electroanal. Chem.* **1991**, *302*, 131−144.

(23) Mussell, R. D.; Nocera, D. G. *J. Am. Chem. Soc.* **1988**, *110*, 2764−2772.

(24) Sartin, M. M.; Shu, C.; Bard, A. J. *J. Am. Chem. Soc.* **2008**, *130*, 5354−5360.

(25) Shen, M.; Rodríguez-López, J.; Huang, J.; Liu, Q.; Zhu, X.-H.; Bard, A. J. *J. Am. Chem. Soc.* **2010**, *132*, 13453−13461.

(26) Fan, F.-R. F.; Cliffel, D.; Bard, A. J. *Anal. Chem.* **1998**, *70*, 2941−2948.

(27) Miao, W.; Choi, J.-P.; Bard, A. J. *J. Am. Chem. Soc.* **2002**, *124*, 14478−14485.

(28) Zu, Y.; Ding, Z.; Zhou, J.; Lee, Y.; Bard, A. J. *Anal. Chem.* **2001**, *73*, 2153−2156.

(29) Kanoufi, F.; Cannes, C.; Zu, Y.; Bard, A. J. *J. Phys. Chem. B* **2001**, *105*, 8951−8962.

(30) Tokel, N. E.; Bard, A. J. *J. Am. Chem. Soc.* **1972**, *94*, 2862−2863.

(31) Rubinstein, I.; Bard, A. J. *J. Am. Chem. Soc.* **1981**, *103*, 512−516.

(32) White, H. S.; Bard, A. J. *J. Am. Chem. Soc.* **1982**, *104*, 6891−6895.

(33) Leland, J. K.; Powell, M. J. *J. Electrochem. Soc.* **1990**, *137*, 3127−3131.

(34) Rodríguez-López, J.; Alpuche-Aviles, M. A.; Bard, A. J. *Anal. Chem.* **2008**, *80*, 1813−1818.

(35) Rodríguez-López, J.; Alpuche-Aviles, M. A.; Bard, A. J. *J. Am. Chem. Soc.* **2008**, *130*, 16985−16995.

(36) Kapturkiewicz, A. *J. Electroanal. Chem.* **1994**, *372*, 101−116.

(37) Shen, M.; Arroyo-Currás, N.; Bard, A. J. *Anal. Chem.* **2011**, *83*, 9082−9085.

(38) Faulkner, L. R.; Tachikawa, H.; Bard, A. J. *J. Am. Chem. Soc.* **1972**, *94*, 691−699.

(39) Zweig, A.; Hoffmann, K.; Maricle, D. L.; Maurer, A. H. *J. Am. Chem. Soc.* **1968**, *90*, 261−268.

(40) Zweig, A.; Maricle, D. L.; Brinen, J. S.; Maurer, A. H. *J. Am. Chem. Soc.* **1967**, *89*, 473−474.

(41) Maricle, D. L.; Maurer, A. *J. Am. Chem. Soc.* **1967**, *89*, 188−189.

(42) Marcus, R. A. *J. Chem. Phys.* **1965**, *43*, 2654−2657.

(43) Chandross, E. A.; Visco, R. E. *J. Phys. Chem.* **1968**, *72*, 378−379.

(44) Juris, A.; Balzani, V.; Barigelletti, F.; Campagna, S.; Belser, P.; Von Zelewsky, A. *Coord. Chem. Rev.* **1988**, *84*, 85−277.

(45) Lakowicz, J. R. *Principles of Fluorescence Spectroscopy*, 3rd ed.; Springer Science + Business Media: New York, NY, 2006.

(46) Gosavi, S.; Marcus, R. A. *Electrochim. Acta* **2003**, *49*, 3−21.

(47) McIntyre, R.; Sass, J. K. *J. Electroanal. Chem.* **1985**, *196*, 199−202.

(48) McIntyre, R.; Sass, J. K. *Phys. Rev. Lett.* **1986**, *56*, 651−654.

(49) Ouyang, J.; Bard, A. J. *J. Phys. Chem.* **1987**, *91*, 4058−4062.

(50) Ouyang, J.; Bard, A. J. *J. Phys. Chem.* **1988**, *92*, 5201−5205.

(51) Murakoshi, K.; Uosaki, K. *J. Phys. Chem.* **1992**, *96*, 4593−4596.

(52) Murakoshi, K.; Uosaki, K. *Phys. Rev. B* **1993**, *47*, 2278−2288.